

Electric and thermal transport properties of topological insulator candidate LiMgBi

Hao OuYang(欧阳豪), Qing-Xin Dong(董庆新), Yi-Fei Huang(黄奕飞), Jun-Sen Xiang(项俊森), Li-Bo Zhang(张黎博), Chen-Sheng Li(李晨圣), Pei-Jie Sun(孙培杰), Zhi-An Ren(任治安), and Gen-Fu Chen(陈根富)

Citation: Chin. Phys. B, 2021, 30 (**12**): 127101. DOI: 10.1088/1674-1056/ac009f
Journal homepage: http://cpb.iphy.ac.cn; http://iopscience.iop.org/cpb

What follows is a list of articles you may be interested in

Anisotropic thermoelectric transport properties in polycrystalline $SnSe_2$

Caiyun Li(李彩云), Wenke He(何文科), Dongyang Wang(王东洋), and Li-Dong Zhao(赵立东)
Chin. Phys. B, 2021, 30 (**6**): 067101. DOI: 10.1088/1674-1056/abeee1

Intercalation of van der Waals layered materials: A route towards engineering of electron correlation

Jingjing Niu(牛晶晶), Wenjie Zhang(章文杰), Zhilin Li(李治林), Sixian Yang(杨嗣贤), Dayu Yan(闫大禹), Shulin Chen(陈树林), Zhepeng Zhang(张哲朋), Yanfeng Zhang(张艳锋), Xinguo Ren(任新国), Peng Gao(高鹏), Youguo Shi(石友国), Dapeng Yu(俞大鹏), Xiaosong Wu(吴孝松)
Chin. Phys. B, 2020, 29 (**9**): 097104. DOI: 10.1088/1674-1056/abab85

Vanadium based XVO_3 (X=Na, K, Rb) as promising thermoelectric materials: First-principle DFT calculations

N A Noor, Nosheen Mushahid, Aslam Khan, Nessrin A. Kattan, Asif Mahmood, Shahid M. Ramay
Chin. Phys. B, 2020, 29 (**9**): 097101. DOI: 10.1088/1674-1056/ab99ad

Single crystal growth, structural and transport properties of bad metal $RhSb_2$

D S Wu(吴德胜), Y T Qian(钱玉婷), Z Y Liu(刘子懿), W Wu(吴伟), Y J Li(李延杰), S H Na(那世航), Y T Shao(邵钰婷), P Zheng(郑萍), G Li(李岗), J G Cheng(程金光), H M Weng(翁红明), J L Luo(雒建林)
Chin. Phys. B, 2020, 29 (**3**): 037101. DOI: 10.1088/1674-1056/ab696e

Magnetism, optical, and thermoelectric response of $CdFe_2O_4$ by using DFT scheme

Q Mahmood, M Yaseen, K C Bhamu, Asif Mahmood, Y Javed, Shahid M Ramay
Chin. Phys. B, 2018, 27 (**3**): 037103. DOI: 10.1088/1674-1056/27/3/037103

Electric and thermal transport properties of topological insulator candidate LiMgBi*

Hao OuYang(欧阳豪)[1,2,†], Qing-Xin Dong(董庆新)[1,2,†], Yi-Fei Huang(黄奕飞)[1,2], Jun-Sen Xiang(项俊森)[1], Li-Bo Zhang(张黎博)[1,2], Chen-Sheng Li(李晨圣)[1,2], Pei-Jie Sun(孙培杰)[1,2,3], Zhi-An Ren(任治安)[1,2,3], and Gen-Fu Chen(陈根富)[1,2,3,‡]

[1] *Institute of Physics, and Beijing National Laboratory for Condensed Matter Physics, Chinese Academy of Sciences, Beijing* 100190, *China*
[2] *School of Physical Sciences, University of Chinese Academy of Sciences, Beijing* 100049, *China*
[3] *Songshan Lake Materials Laboratory, Dongguan* 523808, *China*

(Received 27 March 2021; revised manuscript received 29 April 2021; accepted manuscript online 13 May 2021)

We report the transport properties of a topological insulator candidate, LiMgBi. The electric resistivity of the title compound exhibits a metal-to-semiconductor-like transition at around 160 K and tends to saturation below 50 K. At low temperatures, the magnetoresistance is up to ∼260% at 9 T and a clear weak antilocalization effect is observed in the low magnetic-field region. The Hall measurement reveals that LiMgBi is a multiband system, where hole-type carriers ($n_h \sim 10^{18}$ cm^{-3}) play a major role in the transport process. Remarkably, LiMgBi possess a large Seebeck coefficient (∼440 μV/K) and a moderate thermal conductivity at room temperature, which indicate that LiMgBi is a promising candidate in thermoelectric applications.

Keywords: thermoelectric, topological insulator, crystal growth

PACS: 71.30.+h, 75.47.–m, 65.40.–b, 81.10.–h **DOI:** 10.1088/1674-1056/ac009f

1. Introduction

Thermoelectric (TE) materials have attracted widespread research interest in the development of potential applications for waste heat-to-electricity conversion, or solid-state refrigeration. The efficiency of thermoelectric energy conversions is characterized by the dimensionless parameter[1] $ZT = S^2\sigma T/\kappa$, where σ, S, T, and κ are the electric conductivity, Seebeck coefficient, Kelvin temperature, and thermal conductivity, respectively. However, the strong coupling[2–4] among S, σ and κ leads to a finite improvement of conversion efficiency, preventing the common use of thermoelectric devices. How to eliminate or weaken the coupling among these three parameters is of great significance for further applications of TE materials. Topological materials are highly expected to do so, namely, decoupling the electron and phonon in transport process,[5–9] due to the topologically protected band structure and unconventional electronic properties, such as the strong spin-orbit coupling (SOC) and the inverted band structure. Indeed, Bi_2Te_3, Bi_2Se_3 and its alloying derivatives, famous for their excellent thermoelectric properties, turn out to be the three-dimensional topological insulators (TIs),[10–12] which inspire us to find other excellent thermoelectric candidates in the nontrivial topological materials.

LiMgBi, which is half-Heusler structured (MgAgAs-type) and crystallizes in the cubic $F\bar{4}3m$ space group, was recently identified as a high symmetry point topological semimetal,[13–15] while the latest first-principles calculations by Sattigeri *et al.*[16] have shown that LiMgBi would be a weak TI or band insulator, which could undergo the topological phase transition and transform into a Dirac semimetal driven by the volume expansive pressure. Additionally, the title compound is also predicted as a promising thermoelectric candidate with a large Seebeck coefficient.[17,18] In this work, we have grown the single crystals of LiMgBi and implemented a detailed study on electric and thermal transport properties on it. Our results reveal that LiMgBi is a TI with a multiband feature, and the hole-type carriers dominate the transport. Moreover, LiMgBi possesses a large Seebeck coefficient and a moderate thermal conductivity at room temperature, which provide a good platform to study thermoelectric properties and make it potential in energy-conversion applications.

2. Experiment

High-quality single crystals of LiMgBi were grown by the self-flux method with an optimized molar ratio of Li:Mg:Bi=1:1:10. Mg and Bi powders were mixed thoroughly in a mortar with pestle. Then the powder was placed into an alumina crucible together with Li flakes, covered with quartz wool and sealed into a quartz tube. The sealed quartz ampoule was heated to 873 K, kept at this temperature for 10 h,

*Project supported by the National Key Research and Development Program of China (Grant No. 2016YFA0300604), the National Natural Science Foundation of China (Grant No. 11874417), and the Strategic Priority Research Program (B) of Chinese Academy of Sciences (Grant No. XDB33010100).

†These authors contributed equally to this work.

‡Corresponding author. E-mail: gfchen@iphy.ac.cn

© 2021 Chinese Physical Society and IOP Publishing Ltd

and then cooled down to 623 K at 2.5 K/h. At this temperature, the quartz ampoule was taken out of the muffle furnace and put into a centrifuge to separate the LiMgBi crystals from the Bi flux, then LiMgBi single crystals with typical size of 4 mm×2 mm×1 mm could be obtained. X-ray diffraction (XRD) patterns of polycrystalline and single crystal were collected by a PANalytical x-ray diffractometer with Cu K_α radiation ($\lambda = 1.541874$ Å) at room temperature. Powder XRD Rietveld refinement was performed using the GSAS program.[19] Electric and thermal transport property measurements were used with four-probe method and mainly carried out in a Quantum Design physical property measurement system (QD PPMS-9T). Particularly, to adopt different sizes of a single crystal sample, we performed the thermal transport measurements on both homemade and QD's puck.

3. Results and discussion

LiMgBi (Fig. 1(a)) adopts a filled zinc-blende-type structure.[20] As shown in Fig. 1(b), the elements Mg and Bi occupied the 4*a* and 4*c* Wyckoff sites, respectively, composing the zinc tetrahedrons frame structure; while Li atoms, located at 4*b* Wyckoff site, fill in the cage as the interstitial atoms and form chain along the [110] direction. Meanwhile, this crystal structure is the same as the Half–Heusler phase (*XYZ*), where Li, Mg, and Bi serve as *X*, *Y*, *Z* elements, respectively. The main panel of Fig. 1(c) shows the powder XRD pattern and Rietveld refinement result of the LiMgBi powder sample. The diffraction patterns can be well indexed using the $F\bar{4}3m$ (No. 216) space group, except some very weak peaks from the residual Bi. The refinement smoothly converges to $R_{wp} = 6.48\%$, $R_p = 4.23\%$, the determined lattice parameter $a = b = c = 6.75$ Å, which is in agreement with the previous result.[21] As shown in the inset of Fig. 1(d), the obtained LiMgBi single crystal is black in color with the metallic luster and has a triangle shape. Single crystal XRD pattern reveals that the natural growth crystal surface is (*h h h*) crystallographic plane.

The temperature-dependent resistivity $\rho_{xx}(T)$ measured on LiMgBi single crystal under several magnetic fields is shown in Fig. 2(a). At zero filed, the resistivity $\rho_{xx}(0)$ first decreases linearly with decreasing temperature, exhibiting a metallic behavior until ∼160 K. Thereafter the resistivity starts to increase, reaching a maximum at about 50 K, and finally drops slightly with further cooling. The metal-to-semiconductor-like transition with a low temperature plateau has often been observed in many topological materials, such as SmB_6[22] Bi_2Te_2Se[23] and Bi_2Te_3,[24] which has been taken as a transport signature of conducting surface states of a TI protected by time reversal symmetry. With applied magnetic fields, the resistivity has a moderate increase above ∼130 K, but shows a drastic up-turn below this temperature. This behavior is very similar to other recognized topological materials, such as LaBi[25] and LaSb.[26]

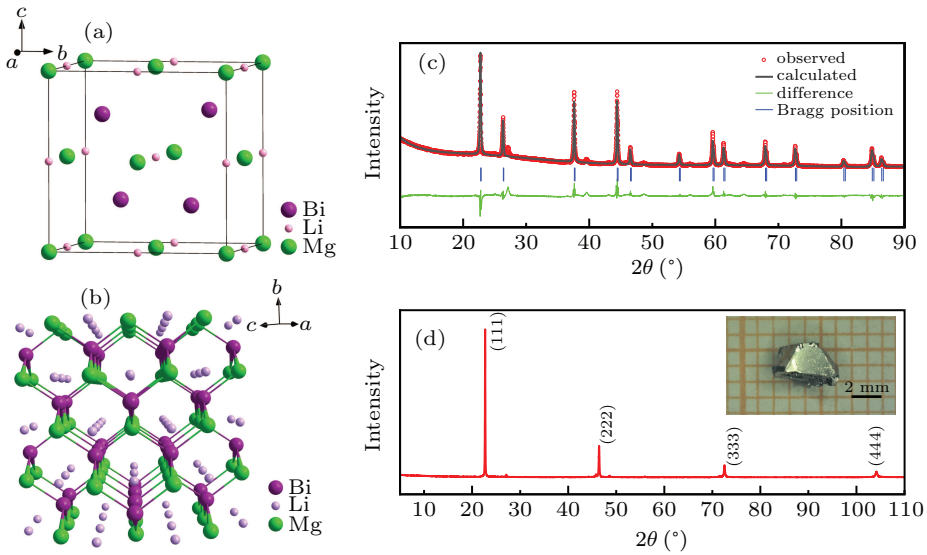


Fig. 1. (a) The crystal structure of LiMgBi. (b) Project view of the lattice along the [110] direction. (c) Powder XRD pattern of LiMgBi and refinements result. (d) Single crystal XRD pattern of LiMgBi. Inset shows the grown crystal on millimeter paper.

The magnetoresistance $\left[\mathrm{MR}(\mu_0 H) = \frac{\rho_{xx}(\mu_0 H) - \rho_{xx}(0)}{\rho_{xx}(0)}\right]$ at various temperatures with applied magnetic fields perpendicular to the current are shown in Fig. 2(b). The magnetoresistance (MR) has slightly change in the temperature region 2–50 K, apart from that the MR decreases fast with the increasing temperature. With the magnetic field increasing to 9 T, the MR reaches ∼260% at 2 K and approaches to saturation. At low fields, the MR increases sharply as the magnetic field increase, which is typically the weak antilocalization (WAL) effect.[27] Hereby we analyzed the MR at 2 K and magnetic field ranging

from −1 T to 1 T using the semiclassical formula[28,29]

$$\sigma(\mu_0 H) = \sigma_{\rm WAL} + \sigma_{\rm N}, \tag{1}$$

$$\sigma_{\rm WAL} = \sigma_0 + a\sqrt{\mu_0 H}, \tag{2}$$

$$\sigma_{\rm N}^{-1} = \rho_0 + A(\mu_0 H)^2, \tag{3}$$

where $\sigma_{\rm WAL}$ and $\sigma_{\rm N}$ are the electric conductivity from the contribution of quantum interference corrections associated with spin orbital scattering and conventional bands; σ_0 and ρ_0 are the electric conductivity and resistivity at zero field. The inset of Fig. 2(b) displayed the experimental data (blue solid dot) and fitting curve (red line) at 2 K. We can see that the low field MR data could be fitted well with the WAL semiclassical formula, which suggests the large intrinsic SOC in LiMgBi arising from Bi. Such behavior is widely observed in some heavy element Bi-based materials.[30–32] Figure 2(c) presents the magnetic field dependence of MR at 2 K for selected angles. There is no significant variation indicating a very weak anisotropy in LiMgBi. To further verify this character, the measurements of angular dependent MR were performed under several magnetic fields at 2 K, as displayed in Fig. 2(d). As the angle changes, the magnetoresistance forms a nearly circular shape, which is consistent with the highly symmetrical cubic crystal structure of LiMgBi.

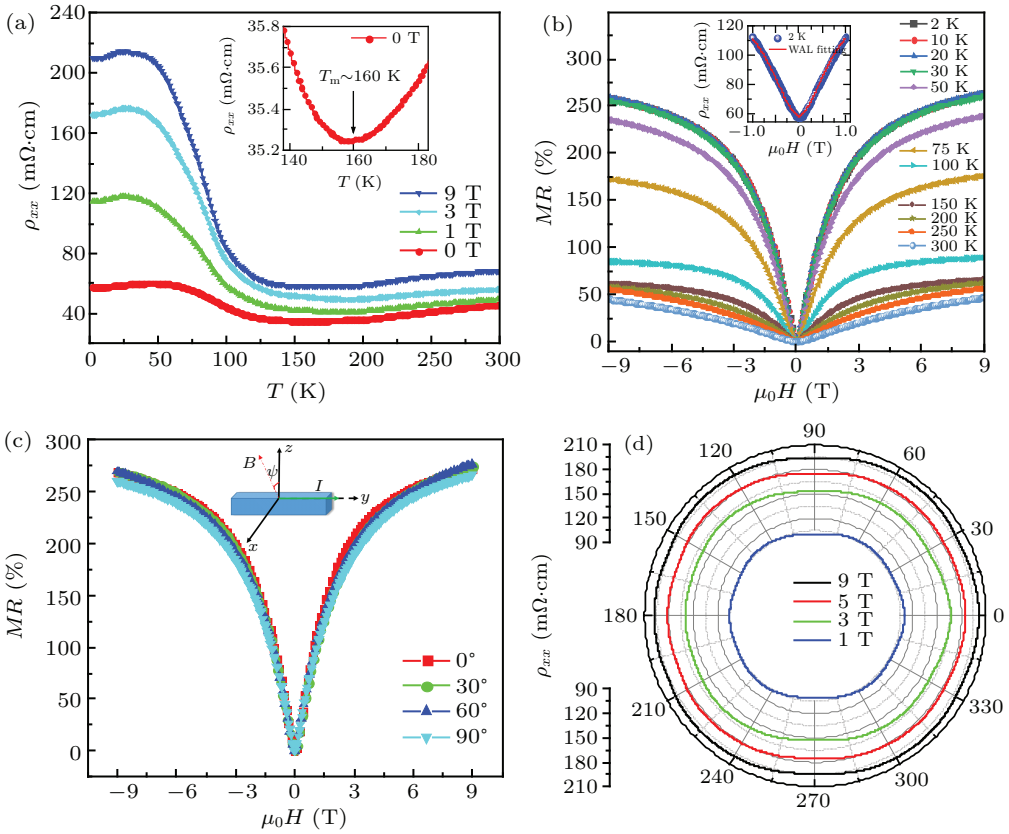


Fig. 2. (a) Temperature dependence of resistivity at different magnetic fields. The electric current is parallel to the (111) plane and magnetic field is perpendicular to the electric current. Inset shows the enlarged part of $\rho_{xx}(T)$ between 140 and 180 K. (b) The MR at various temperatures for magnetic field is perpendicular to (h h h) plane. Inset: the weak antilocalization effect fitting between −1 and 1 T, at 2 K. The blue dots and the red line represent the experimental data and the fitting curve, respectively. (c) Magnetic field dependence of MR at selected angular 2 K with magnetic field rotated in the plane perpendicular to the current for $I \parallel y$. Here ψ is defined as the angle between B and z-axis. (d) Angular dependent MR with keeping magnetic field perpendicular to electric current, at 2 K for selected magnetic field.

We performed Hall measurement at various temperatures for the purpose of investigating the different type carrier's contribution to transport process in this system, as shown in Fig. 3(a). Evidently, the positive Hall coefficient $R_{xy} = \rho_{xy}(\mu_0 H)/B$ within the measured temperature range indicates that hole-type carriers are dominant in the transport process. Furthermore, the deviation from the linear behavior of the Hall resistivity at low fields implies that LiMgBi is a multiband system. Thus, according to the above results, we analyzed the Hall resistivity $\rho_{xy}(\mu_0 H)$ using the semiclassical two-band model with the following formula:

$$\rho_{xy}(\mu_0 H) = \frac{\mu_0 H}{e} \frac{(n_{\rm h}\mu_{\rm h}^2 - n_{\rm e}\mu_{\rm e}^2) + (n_{\rm h} - n_{\rm e})(\mu_{\rm h}\mu_{\rm e})^2 (\mu_0 H)^2}{(n_{\rm h}\mu_{\rm h} + n_{\rm e}\mu_{\rm e})^2 + (n_{\rm h} - n_{\rm e})^2 (\mu_{\rm h}\mu_{\rm e})^2 (\mu_0 H)^2}, \tag{4}$$

where $n_{\rm e}$, $\mu_{\rm e}$, $n_{\rm h}$, $\mu_{\rm h}$ are the carrier density and mobility of electron and hole, respectively. The temperature dependences of the carrier density and mobility extracted from the Hall resistivity fitting are shown in Figs. 3(b) and 3(c). The estimated $n_{\rm e}$, $n_{\rm h}$, $\mu_{\rm e}$, $\mu_{\rm h}$ at 2 K are 1.07×10^{14} cm^{-3}, 3.86×10^{18} cm^{-3}, 5.37×10^{3} cm^2/(V·s), 0.02×10^{3} cm^2/(V·s),

respectively. When the temperature increases, the hole density increases while the electron density is substantially unchanged below 50 K. As the temperature rises further, the hole density decreases significantly together with a sharp increasing of electron density until both of them reach the minimum (1.18×10^{18} cm^{-3} for hole) and maximum (3.52×10^{14} cm^{-3} for electron) values at 200 K. Additionally, the evolution trends of hole mobility (0.06×10^3 cm^2/(V·s) the maximum at $\sim$ 200 K) is the same as that of electron density. The electron mobility has a slight augment below 50 K, but a continuous decrease until room temperature (2.06×10^3 cm^2/(V·s) at 300 K). Remarkably, the density of hole-type carries is in order of 10^{18} cm^{-3}, which have the same magnitude order as typical TI materials, such as $Bi_{1-x}Sb_x$,[33] Sb_2Te_3.[12,34] It is two or even more orders of magnitude lower than the carrier density of typical topological semimetals (10^{20}–10^{21} cm^{-3}) such as WC,[35] WTe_2,[36] and gray As,[37] which implies that LiMgBi prefers to be a TI rather than a topological semimetal. Noticeably, the hole density is four orders of magnitude larger than that of electron in all measured temperature range, it is reasonable that the transport properties are dominated by holes, and the high mobility of electron (two orders of magnitude larger than that of hole) may originate from the nontrivial topological metallic surface state, similar to Bi_2Se_3.[38,39]

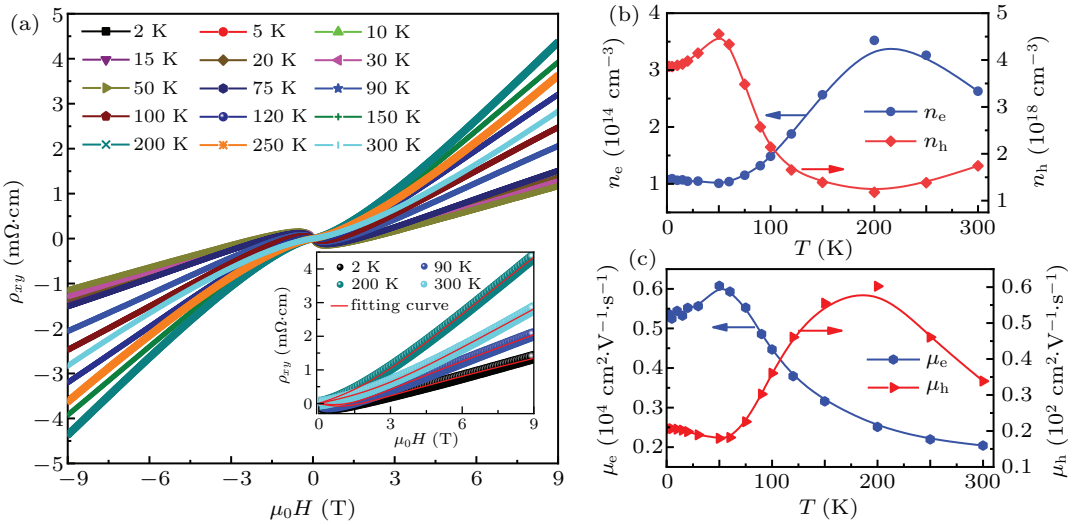


Fig. 3. (a) The magnetic field dependent Hall resistivity at various temperatures. Inset: two-band model fitting of $\rho_{xy}(\mu_0 H)$ at selected temperatures. (b) and (c) The density and mobility of electron and hole versus temperature, respectively.

In order to evaluate the potential of the utilization of this thermoelectric candidate, we performed the thermoelectric transport measurements on the polycrystalline and single crystal of LiMgBi, respectively, as presented in Fig. 4. As the temperature rises, the single crystal Seebeck coefficient of LiMgBi increases rapidly from 21.6 μV/K at 2 K to 380.7 μV/K at 75 K, and then undergoes a moderate ascension up to 440 μV/K at room temperature after the stationary range. By contrast, the Seebeck coefficient of the polycrystalline is basically temperature independent below 125 K and begins to increase enormously and reaches the maximum of 276.1 μV/K at 363 K. The difference of Seebeck coefficient between single crystal and polycrystalline should be attributed to the influence of grain boundaries scattering or carries densities.[40,41] In addition, both of them exhibit positive values in the measurement temperature range, further confirming that the hole-type carries play a dominant role in the thermoelectric transport process, and the derailment from linearly increasing behavior also verifies the multiband system. Figure 4(b) presents the thermal conductivity κ of LiMgBi polycrystalline and single crystal. The thermal conductivity of single crystal has a tremendous variation. As the temperature rises, it quickly reaches the peak (68.1 W·K^{-1}·m^{-1} at 12 K) and then drops rapidly to the 5.2 W·K^{-1}·m^{-1} at 300 K. On the contrary, the thermal conductivity of polycrystalline always maintains a steady change between 2 and 3 W·K^{-1}·m^{-1} when temperature is above 100 K. The weak upturn may come from heat radiation at high temperatures. The inset of Fig. 4(b) shows the comparison of total thermal conductivity κ_{tot} and electron portion κ_e for single crystal, which can be extracted from the κ_{tot} using the Wiedemann–Franz (W-F) law

$$\frac{\kappa_e}{T} = \sigma L_0, \tag{5}$$

where L_0 is Lorenz number (2.44×10^{-8} W·Ω·K^{-2}), σ is the electric conductivity and T is Kelvin temperature. It can be seen the κ_e is almost three orders of magnitude smaller than κ_{tot}, indicating that the most contribution to the transport of heat is mainly derived from lattice thermal conductivity. There are a lot of margins to reach the amorphous limit to further improve thermoelectric performance.

What we should pay attention to are the following points: (1) The large Seebeck coefficient. LiMgBi possesses the large

Seebeck coefficient ~440 μV/K at 300 K, it is even larger than that of the optimized traditional commercial alloy of $Bi_2Te_3$and Sb_2Te_3[42] (~ 230 μV/K at 300 K). What's more noteworthy is that it maintains continuously the large thermoelectric coefficient value in a wide range (above 75 K). (2) The comparable thermal conductivity (5.2 $W \cdot K^{-1} \cdot m^{-1}$ at 300 K) with Sb_2Te_3[42] (~ 4.5 $W \cdot K^{-1} \cdot m^{-1}$ at 300 K) and SiGe (~ 3 $W \cdot K^{-1} \cdot m^{-1}$ at 300 K)[43] inspire us to optimize the thermal conductivity by doping, nanosizing and thin-film superlattices or other methods to enhance the thermoelectric performance. (3) Unique properties of topological materials. LiMgBi, a TI candidate, has the unconventional electronic structure and specific electronic properties, and it is possible to considerably decouple the electron and phonon transport, reducing its lattice thermal conductivity while retaining the moderate electric conductivity of topological metallic surface states. Therefore, LiMgBi provides a good topological material platform to enhance thermoelectric performance.

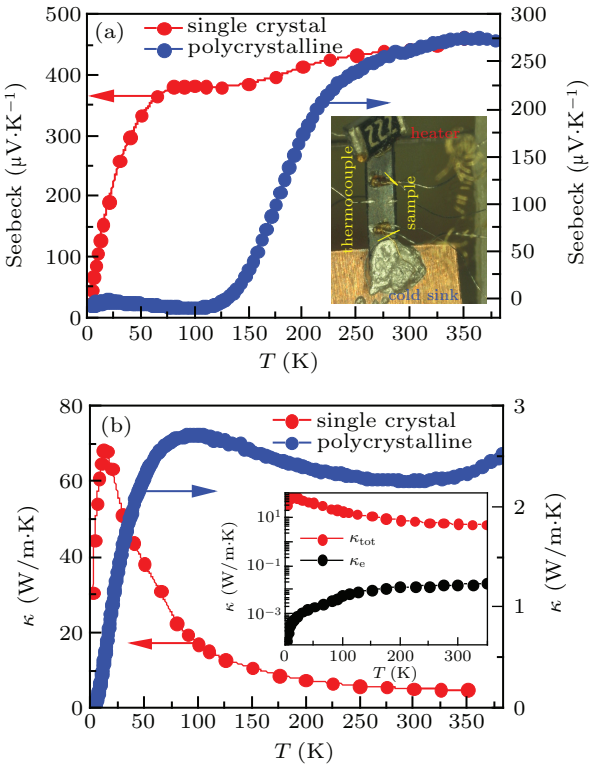


Fig. 4. (a) and (b) The temperature dependence of Seebeck coefficient and thermal conductivity for single crystal and polycrystalline of LiMgBi. Inset: the photo image of the sample mounted on a sample holder. (Single crystal and polycrystalline measurement are performed on homemade instrument and QD-PPMS 9T).

4. Conclusion

In summary, we have successfully grown the single crystals of LiMgBi and its electric and thermal transport properties have been studied systematically. The electric resistivity shows a metal-to-semiconductor-like transition at ~160 K. While below 50 K, the resistivity tends to saturation, which may be rooting in the competition between bulk state and topological metallic surface state. The WAL effect was clearly observed in MR measurements, implying the large intrinsic SOC in LiMgBi. Hall measurements indicate that LiMgBi is a multiband system, which is dominated by the hole-type carriers in the transport process. The thermoelectric transport measurement states clearly a larger Seebeck coefficient (~440 μV/K) and a moderate thermal conductivity, which are worthy of further studies to assess the potential as a thermoelectric material candidate.

References

[1] Goldsmid H J 2010 *Introduction to Thermoelectricity* (Berlin: Springer) p. 46
[2] Tritt T M and Subramanian M A 2006 *MRS Bull.* **31** 188
[3] DiSalvo F J 1999 *Science* **285** 703
[4] Rowe D M 2018 *CRC Handbook of Thermoelectrics* (New York: CRC Press)
[5] Müchler L, Casper F, Yan B, Chadov S and Felser C 2013 *Phys. Status Solidi RRL* **7** 91
[6] Takahashi R and Murakami S 2012 *Semicond Sci. Technol.* **27** 124005
[7] Xu Y 2016 *Chin. Phys. B* **25** 117309
[8] Fu C, Sun Y and Felser C 2020 *APL Mater.* **8** 040913
[9] Xu N, Xu Y and Zhu J 2017 *npj Quantum Mater.* **2** 1
[10] Poudel B, Hao Q, Ma Y, Lan Y C, Minnich A, Yu B, Yan X A, Wang D Z, Muto A, Vashaee D, Chen X Y, Liu J M, Dresselhaus M S, Chen G and Ren Z F 2008 *Science* **320** 634
[11] Chen Y L, Analytis J G, Chu J H, Liu Z K, Mo S K, Qi X L, Zhang H J, Lu D H, Dai X, Fang Z, Zhang S C, Fisher I R, Hussain Z and Shen Z X 2009 *Science* **325** 178
[12] Zhang H J, Liu C X, Qi X L, Dai X, Fang Z and Zhang S C 2009 *Nat. Phys.* **5** 438
[13] Vergniory M G, Elcoro L, Felser C, Regnault N, Bernevig B A and Wang Z 2019 *Nature* **566** 480
[14] Bradlyn B, Elcoro L, Cano J, Vergniory M G, Wang Z, Felser C, Aroyo M I and Bernevig B A 2017 *Nature* **547** 298
[15] Tang F, Po H C and Vishwanath A and Wan X 2019 *Nature* **566** 486
[16] Sattigeri R M, Pillai S B, Jha P K and Chakraborty B 2020 *Phys. Chem. Phys.* **22** 4602
[17] Yadav M K and Sanyal B 2015 *J. Alloys Compd.* **622** 388
[18] Parsamehr S, Boochani A, Amiri M, Solaymani S, Sartipi E, Naderi S and Aminian A 2020 *Philos. Mag.* **101** 369
[19] Toby B H 2001 *J. Appl. Crystall.* **34** 210
[20] Bende D, Grin Y and Wagner F R 2014 *Chemistry* **20** 9702
[21] Nowotny H and Holub F 1960 **91** 877
[22] Zhang X, Sun S S and Lei H C 2017 *Phys. Rev. B* **95** 035209
[23] Ren Z, Taskin A, Sasaki S, Segawa K and Ando Y 2010 *Phys. Rev. B* **82** 241306
[24] Qu D X, Hor Y S, Xiong J, Cava R J and Ong N P 2010 *Science* **329** 821
[25] Sun S, Wang Q, Guo P J, Liu K and Lei H C 2016 *New J. Phys.* **18** 082002
[26] Tafti F, Gibson Q D, Kushwaha S K, Haldolaarachchige N and Cava R J 2016 *Nat. Phys.* **12** 272
[27] Checkelsky J G, Hor Y S, Cava R J and Ong N P 2011 *Phys. Rev Lett.* **106** 196801
[28] Xiong J, Kushwaha S K, Liang T, Krizan J W, Hirschberger M, Wang W D, Cava R J and Ong N P 2015 *Science* **350** 413
[29] Huang X C, Zhao L X, Long Y J, Wang P, Chen D, Yang Z H, Liang H, Xue M Q, Weng H M, Fang Z, Dai X and Chen G F 2015 *Phys. Rev. X* **5** 031023
[30] Isaeva A, Rasche B and Ruck M 2013 *Phys. Status Solidi RRL* **7** 39
[31] Xia Y, Qian D, Hsieh D, Wray L, Pal A, Lin H, Bansil A, Grauer D, Hor Y S, Cava R J and Hasan M Z 2009 *Nat. Phys.* **5** 398
[32] Murakami S 2006 *Phys. Rev. Lett.* **97** 236805
[33] Syers P and Paglione J 2017 *Phys. Rev. B* **95** 045123

[34] Harman T C, Paris B, Miller S E and Goering H L 1957 *J. Phys. Chem. Solids* **2** 181
[35] He J B, Chen D, Zhu W L, Zhang S, Zhao L X, Ren Z A and Chen G F 2017 *Phys. Rev. B* **95** 195165
[36] Luo Y K, Li H, Dai Y M, Miao H, Shi Y G, Ding H, Taylor A J, Yarotski D A, Prasankumar R P and Thompson J D 2015 *Appl. Phys. Lett.* **107** 182411
[37] Zhao L X, Xu Q N, Wang X M, He J B, Li J, Yang H X, Long Y J, Chen D, Liang H, Li C H, Xue M Q, Li J Q, Ren Z A, Lu L, Weng H M, Fang Z, Dai X and Chen G F 2017 *Phys. Rev B* **95** 115119
[38] Shrestha K, Chou M, Graf D, Yang H D, Lorenz B and Chu C W 2017 *Phys. Rev. B* **95** 195113
[39] Butch N P, Kirshenbaum K, Syers P, Sushkov A B, Jenkins G S, Drew H D and Paglione J 2010 *Phys. Rev. B* **81** 241301
[40] Mi H X, Li H Y, Qiao C Y, Zhang T, Han L and Xu J 2020 *Rare Metal. Mat. Eng.* **49** 2234
[41] Gao Y W, He Y Z and Zhu L L 2010 *Chin. Sci. Bull.* **55** 16
[42] Champness C H, Chiang P T and Parekh P 1965 *Can. J. Phys.* **43** 653
[43] Snyder G J and Toberer E S 2008 *Nat. Mater.* **7** 105